University of Bath

Alternative formats

If you require this document in an alternative format, please contact:
openaccess@bath.ac.uk

Accepted Manuscript

Evaluation of seabed mapping methods for fine-scale classification of extremely shallow benthic habitats – Application to the Venice Lagoon, Italy

G. Montereale Gavazzi, F. Madricardo, L. Janowski, A. Kruss, P. Blondel, M. Sigovini, F. Foglini
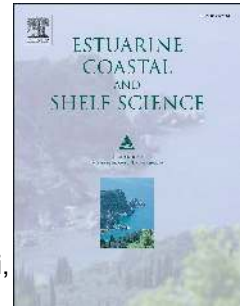
Please cite this article as: Montereale Gavazzi, G., Madricardo, F., Janowski, L., Kruss, A., Blondel, P., Sigovini, M., Foglini, F., Evaluation of seabed mapping methods for fine-scale classification of extremely shallow benthic habitats – Application to the Venice Lagoon, Italy, *Estuarine, Coastal and Shelf Science* (2016), doi: 10.1016/j.ecss.2015.12.014.

Evaluation of seabed mapping methods for fine-scale classification of extremely shallow benthic habitats – Application to the Venice Lagoon, Italy

Montereale Gavazzi, G. [a,*] , Madricardo, F. [a], Janowski, L. [b], Kruss, A. [a], Blondel, P. [c] , G., Sigovini, M. [a], Foglini, F. [d],

[a] Istituto di Scienze Marine-Consiglio Nazionale delle Ricerche, Arsenale - Tesa 104, Castello 2737/F, 30122 Venezia, Italy

[b] Institute of Oceanography, University of Gdansk, al. Marszalka Pilsudskiego 46

81-378 Gdynia, Poland

[c] Department of Physics, University of Bath, Bath BA2 7AY, United Kingdom

[d] Istituto di Scienze Marine-Consiglio Nazionale delle Ricerche, Bologna, Italy

[*] Corresponding Author: Tel.: (+39) 041 2407986, Fax: (+39) 041 2407940, E-mail: giacomo.montereale@ve.ismar.cnr.it

Abstract

Recent technological developments of multibeam echosounder systems (MBES) allow mapping of benthic habitats with unprecedented detail. MBES can now be employed in extremely shallow waters, challenging data acquisition (as these instruments were often designed for deeper waters) and data interpretation (honed on datasets with resolution sometimes orders of magnitude lower). With extremely high-resolution bathymetry and co-located backscatter data, it is now possible to map the spatial distribution of fine scale benthic habitats, even identifying the acoustic signatures of single sponges. In this context, it is necessary to understand which of the commonly used segmentation methods is best suited to account for such level of detail. At the same time, new sampling protocols for precisely geo-referenced ground truth data need to be developed to validate the benthic environmental classification. This study focuses on a dataset collected in a shallow (2–10 m deep) tidal channel of the Lagoon of Venice, Italy. Using 0.05-m and 0.2-m raster grids, we compared a range of classifications, both pixel- based and object-based approaches, including manual, Maximum Likelihood Classifier, Jenks Optimization clustering, textural analysis and Object Based Image Analysis. Through a comprehensive and accurately geo-referenced ground truth dataset, we were able to identify five different classes of the substrate composition, including sponges, mixed submerged aquatic vegetation, mixed detritic bottom (fine and coarse) and unconsolidated bare sediment. We computed estimates of accuracy (namely Overall, User

and Producer Accuracies) by cross tabulating predicted and reference instances. Overall, pixel based segmentations produced the highest accuracies and that the accuracy assessment is strongly dependent on the choice of classes for the segmentation. Tidal channels in the Venice Lagoon are extremely important in terms of habitats and sediment distribution, particularly within the context of the new tidal barrier being built. However, they had remained largely unexplored until now, because of the surveying challenges. The application of this remote sensing approach, combined with targeted sampling, opens a new perspective in the monitoring of benthic habitats in view of a knowledge-based management of natural resources in shallow coastal areas.

Keywords: *Benthic habitat mapping, high-resolution sonar, image segmentation, very shallow water, multibeam, Venice Lagoon*

1.   Introduction

Estuaries and coastal ecosystems are amongst the most productive and valuable environments on Earth (Guelorget and Perthuisot, 1992, Costanza et al., 1997, Barbier et al. 2011, Kirwan and Megonigal, 2013). These ecosystems are particularly susceptible to anthropogenic pressure, with 13 of the 15 world biggest cities located close to the coast (Kennish, 2000; McGlathery et al., 2007; Halpern et al., 2008; Brown and Blondel, 2009). Large national and international programs have started to map these ecosystems, e.g. *Mapping European Seabed Habitats* (*MESH*) (http://www.searchmesh.net), *MESH Atlantic* (http://www.meshatlantic.eu), *EU Seamap* (http://jncc.defra.gov.uk/page-5040), *MAREANO* (http://mareano.no/en), *UK SeaMap* (McBreen et al., 2011), the Irish *INFOMAR* program (http://www.infomar.ie), the *Gulf of Maine Mapping Initiative* (http://www.gulfofmaine.org/gommi), the *Victorian marine habitat mapping project* in Australia (http://hdl.handle.net/10536/DRO/DU:30010514). Accurate mapping of seafloor geomorphology and composition is the basis of marine spatial planning and the implementation of fact-based legislative frameworks (e.g. for the designation of Marine Protected Areas). However, currently, only 5 to 10% of the seabed has been mapped in detail, the majority of which is deeper than 10 m (Blondel, 2009; NOAA, 2014). This is a concern, particularly in view of European legislative frameworks (i.e. Water Framework Directive, 2000: 60/EC; Marine Strategy Framework Directive, 2008/56/EC; Habitats Directive, 92/43/EEC), as an estimate (based on the EMODNet (2015) bathymetry portal data) shows that 9% of EU coastal waters (bathymetry up to 100 m) are shallower than 10 m.

In the present analyses, we consider habitats as including the physical and environmental conditions (mainly of the seafloor) together with the co-inhabitant biota at a given scale (in line with the definitions set forth by Udvardy, 1959, *inter alia*, and in line with the recommendations set by MESH, 2008). The exploration and mapping of coastal and shallow benthic habitats (depths < 30 m) is significantly limited if using conventional surveying technologies. Satellite and aerial remote sensing techniques have been employed to map the broad-scale spatial organization of littoral ecosystems (e.g. Wang and Philpot, 2007), although water turbidity and lowered light penetration strongly restrict the potential of such applications (Lehman and Lachavanne, 1997, Blondel, 2012). Conversely, acoustic remote sensing techniques are constrained by the shallow depths, which limit available coverage away from the surveying platforms and can be affected by strong multiple reflections from the sea surface if using systems designed for deeper waters. Recent developments in underwater acoustic technology can now produce results with a resolution approaching that of photography. Benthic habitat maps based on acoustic data are now commonly used within the context of ecosystem-based management (e.g. Ierodiaconou, 2007, Erdey-Heydorn, 2008, Ierodiaconou, 2011 Brown et al. 2011, Lucieer et al. 2013).

In particular, multibeam echo sounder systems (MBES) allow co-registering bathymetry and backscatter data. MBES can be designed to operate at very high frequencies (up to 400 kHz) and with tuneable pulse lengths and repetitions, yielding high-resolution measurements over relatively large areas of the seabed (Kenny et al. 2003, Parnum and Gavrilov, 2011). High-resolution MBES has led to a better detection of benthic habitats *sensu lato,* allowing a continuous fine-scale mapping of their distribution (Brown et al. 2011). Whilst MBES have been used extensively in shallow and deep waters, their application in very shallow waters (herein defined as < 10 m depth) is only very recent (e.g. Huvenne et al., 2007; De Falco et al., 2010, Micallef et al., 2012).

In this study, we use very high-resolution MBES data (0.05- and 0.2- m grids), combined with *in situ* observations to map and classify a very shallow benthic environment in the Lagoon of Venice. This lagoon is the largest in the Mediterranean (about 550 km², with a mean depth of only 1.2 m). Its tidal channels are virtually unexplored systems with high biodiversity and distinctive biotic communities (Vatova, 1940, Occhipinti-Ambrogi, 2000, Corriero et al., 2007, Sigovini et al., 2014). Up to now, most of the benthic research has been carried out in the mud-flats (e.g. Tagliapetra et al., 1998; Pranovi et al., 2000; Sfriso et al., 2001; Maggiore et al., 2007) which account for the largest lagoon surface area and are logistically easier to access and sample. Tidal channels occupy 15% of the open-lagoon

3

surface with an area of about 64 km². Their depths range from less than 1 m up to a maximum of 50 m.

The combination of large areas and very high resolution data justifies the use of automated habitat classification. There have been fast and recent developments in integrating analyses of the acoustic data (bathymetry and/or imagery) with available ground truth, and different manners of presenting habitat maps have been proposed (see Brown et al., 2011, for a review). Promising quantitative and objective new approaches have been developed, using mixed methods, i.e. pixel-, field and object-based image analyses) (e.g. Brown and Blondel, 2009; Brown et al., 2011, Ierodiaconou et al., 2011; Lucieer and Lamarche, 2011; Micallef et al., 2012; Diesing et al., 2014; McGonigle and Collier, 2014).

However, there have been very few comparisons (e.g. Diesing et al., 2014; Calvert et al., 2014; Galparsoro et al., 2015), all focusing on lower-resolution (> 1 m) data. The very high grid resolutions (< 5 cm) afforded by new systems and new applications, like in the Lagoon of Venice, are setting new challenges for benthic habitat mapping.

In the present study, we apply a few different methods well-established in the realm of classification of remotely sensed data. They were chosen either because of their widespread availability within commercial and open access GIS platforms or because they were successfully applied before. In our choice, we considered both backscatter intensity and textural parameter methods, to see which image characteristic is best to identify the seafloor types of interest. Our aim is therefore to assess which backscatter segmentation method is most suitable to map very fine scale, heterogeneous benthic habitats. At the same time, we investigate the effect of pixel size at varying resolutions (i.e. 0.05 and 0.2 m) on classification results. This is supplemented with a combination of ground truth information including free-diving observations, underwater photography and video and benthos samples at the most relevant points.

2.   Material and Methods

2.1   Study Site

The study site is located in the northern part of the Venice Lagoon, Italy (Fig. 1). The Scanello channel is a natural tidal channel, part of a complex tidal system of tidal creeks and coastal salt marshes. The channel flows as a side-branch of a main navigation channel into a salt marsh area. The channel shows an erosion-deposition pattern characteristic of meandering tidal channels (Perrillo, 2009). The channel follows a gentle sloping gradient from north to south. Its bathymetry is complex, with geomorphologic features like scours, ripple-like structures, flat zones, point bars and pools (Darlymple and Rhodes, 1995).

Following a short straight section of about 200 m, the channel bends to the North for about 300 m, where it separates into two smaller branches flowing into an extremely shallow tidal flat with depths < 1 m. These branches are characterized by the relative highest ruggedness, quantified with the Benthic Terrain Modeler for ArcGIS (Wright et al. 2005, Lundblad et al., 2006) as a Vector Ruggedness Measure (VRM) between 3×10^{-3} and 10^{-2} (Fig. 1C). Their VRM isotropic distribution suggests the presence of biogenic features (Ferrini and Flood, 2006). The dune-like fields in the main branch of the channel also have a high ruggedness. Conversely, the rest of the channel is quite smooth (VRM ruggedness between 10^{-5} and 3×10^{-3}).

2.2. Data acquisition and processing

2.2.1. Geophysical data

Bathymetry and backscatter imagery of the Scanello channel were acquired in November 2013 with a Kongsberg EM-2040 DC dual-head system. The MBES was pole-mounted on the vessel *RV Litus*, a 10-m long boat with 1.5-m draft. The MBES has 800 beams (400 per swath) and a frequency that can range from 200 to 400 kHz. During the survey, the frequency was set to 360 kHz. This was the highest frequency that allowed overlapping of the dual-head system swaths, including in extremely shallow waters. A Seapath 300 positioning system was used with a Fugro HP differential Global Positioning System (DGPS, accurate to 0.20 m) and motion unit to register pitch, roll, heave and yaw corrections (0.02° roll and pitch accuracy, 0.075° heading accuracy). The sound velocity was measured continuously with a Valeport mini SVS sensor close to the transducers. During the survey, sound velocity profiles were also collected with an AML oceanographic Smart-X sound velocity profiler. Data logging, real-time quality control and real-time display were carried out with the Kongsberg native data acquisition and control software SIS (Seafloor Information System). Tidal corrections were obtained using the hydrodynamic model SHYFEM, which models the values of water level all over the lagoon (Umgiesser et al., 2004). It computes the sea level at each virtual tide gauge using the wind and sea level data from all tidal stations in the lagoon and at the inlets, resulting in errors < 0.01 m. All the corrections are referred to the local datum Punta Salute 1897. CARIS HIPS and SIPS (v8.1) were used to account for sound velocity variations, tides and basic quality controls in the derivation of bathymetric data. Backscatter mosaics were created combining the georeferenced backscatter rasters (GeoBaR) of each survey line generated by the Geocoder algorithm that corrects the system settings, transmission loss, insonification area and incidence angle (Fonseca and Calder, 2005). GeoBaRs were produced

after applying to the raw backscatter data the CARIS adaptive Angle Varying Gain (AVG) correction to remove the angular artefacts of sediment from the imagery and the Despeckle option to remove isolated pixels (Caris, 2009). The bathymetric grids and backscatter mosaics were exported from CARIS as text files with grid resolutions of 0.05 and 0.2 m. They were converted to 32-bit raster files using *R* (`raster Package` by Hijmans et al. 2014). The raster files were then imported in ArcGIS (v10.2) (ESRI 2015) for further analysis.

2.2.1.1. Manual segmentation

The backscatter images have a dynamic range of *NG* grey levels, forming a complex, multifaceted mosaic characterized by distinct spatial arrangements of acoustic reflectivities. A visual discrimination of the backscatter imagery and the bathymetry and its derivatives was carried out to identify spatially homogenous units. By digitizing the borders of these acoustic regions of the study area, we obtained two classified vector polygon layers. Two hierarchical levels were defined and mapped: (i) Large spatially homogenous "acoustic macro-regions" (area > 5 m^2) and (ii) small (area < 5 m^2) acoustic objects.

2.2.1.2. Texture analysis with TexAn

Grey Level Co-occurrence Matrices (GLCMs) have been shown to be the most adaptable tools for textural analyses of sonar imagery (Blondel, 1996, 2000; Gao et al., 1998; Micallef et al., 2012). GLCMs express the relative frequency of occurrence $P_D(i,j)$ of two points, with respective grey levels i and j, at Euclidean distances D from each other (D is the inter-pixel displacement). Co-occurrences were averaged over all orientations (by 45° steps). Two textural indices, entropy and homogeneity, are sufficient to describe the GLCMs and resolve most textures visible in sonar imagery (Blondel, 1996; Blondel et al., 1998; Blondel and Gómez Sichi, 2009). Entropy measures the lack of spatial organisation inside the computation window, akin to roughness, whereas homogeneity quantifies the amount of local dissimilarities inside the computation window (Blondel, 1996), i.e. the local organisation. Textural analyses were carried out using the software TexAn (Blondel, 2000; Blondel and Gómez Sichi, 2009).

The MBES mosaic was converted to 8-bit grey levels (0 to 255), by linear scaling from the calibrated backscatter levels (- 40 dB to -5 dB), yielding 0.13 dB per grey level. This had the effect of smoothing out small dB variations of no physical significance, especially considering typical MBES accuracy (≤ 1 dB). TexAn parameters were optimized to separate the distinctive backscatter signatures identified in Table 1, according to their respective entropy and homogeneity values. This was investigated by varying *NG* from 256 down to 8

grey levels, and calculating GLCMs over square windows of length *WD* (from 10 to 80 pixels, by increasing steps of 10 pixels), systematically varying *D* from 5 to (*WD* – 5) pixels. The entropy and homogeneity grids were in turn exported as 8-bit rasters. The final classification was obtained by applying the Maximum Likelihood Classifier (MLC) (in ArcGIS-v10.2) to these rasters and to the 3x3 mean filtered backscatter grid.

2.2.1.3. Jenks' Optimization clustering

The Jenks' Optimization clustering is an easy to implement tool in ArcGIS (v10.2) to classify rasters. Given a certain number of classes, the method seeks to reduce the variance within classes and maximize the variance between classes. From the ground truth dataset, we visually derived five habitat classes (*sensu lato*) (Table 1). To assess the optimal number of backscatter clusters independently, we computed the Jenks classification (also referred to as Fisher-Jenks algorithm) altering *k* (number of classes) from 2 to 6 with the R Package `ClassInt` (Bivand et al. 2009). This procedure is similar to computing the Within Group Sum of Squared Distances plot in a K-Means cluster analysis. We then compared the partitions by deriving the Goodness of Variance Fit (GVF) index finding that five classes gave optimal fit. We then applied Jenks' Optimization clustering in ArcGIS (v10.2) to both datasets.

However, per-pixel classifiers may cluster together disparate features "looking and sounding the same" as pointed out by Lucieer et al., (2013) amongst others. In our case, the class of lowest backscatter groups together large patches (> 1 m²) and small objects (< 1 m²) representing different seafloor properties. To overcome this problem, we converted this backscatter class into polygon features. By querying polygon size (with a threshold of 1 m²), after applying a 3×3 mean filter, we separated small and roughly circular backscatter objects from large patches of very low backscatter.

2.2.1.4. Maximum Likelihood Classifier

The MLC is amongst the most firmly established pixel-based parametric algorithms of remotely sensed imagery classification (Lu and Weng, 2007). Assuming a Gaussian distribution of the data, the algorithm partitions the dataset into groups defined by a given set of training samples. The MLC calculates the class membership probability and assigns each pixel to the group having the highest membership probability. Mean and covariance are extrapolated from the training samples.

7

We used the Maximum Likelihood Classifier Tool in the Spatial Analyst Toolbox in ArcGIS (v10.2) to perform a per-field supervised classification. Similarly to Seo et al. (2014), we digitised a set of training fields (parcels) over the ground truth locations (digitisation of field records). Given the spatial homogeneity of the backscatter patches surrounding the ground truth locations we used 1-m² square polygon fields to map all classes except the sponge class, for which circular and irregular fields were used. Signature files were produced using the Create Signature Tool in ArcGIS. Hierarchical Cluster Analysis was used to assess the dissimilarity of the training samples.

2.2.1.5. Object Based Image Analysis with eCognition

Object based-image analysis (OBIA) is a relatively novel application to remotely sensed seafloor data, with several studies showing its potential (Lucieer and Lamarche, 2011; Diesing et al. 2014). OBIA is a two-step image processing technique that involves segmentation and classification. The segmentation separates the image into image objects of variable sizes, based on their spectral and spatial characteristics. The maximum allowed heterogeneity for the segmented objects defines the scale and constrains their dimensions. In turn, the objects are classified using different algorithms (Benz et al., 2004). This analysis was carried out with the eCognition© software, using multibeam backscatter with resolutions of 0.05 m and 0.2 m. After trying different scale values for the multiresolution segmentation, we found the best results by setting the scale to 5 and 15 for the 0.05 m and the 0.2 m resolution images, respectively. The image object Shape was set to 0.1 and Compactness to 0.5 in accordance with Lucieer et al. (2013) and Stephen and Diesing (2014). The value of the Shape parameter can range from 0.1 to 0.9 and defines the proportion between colour and shape criteria of homogenous area. Shape 0.1 means that the objects are more optimized for backscatter intensity than for its spatial homogeneity. Another parameter, compactness measures the ratio between the image object border length and the root mean square (RMS) of all pixel values within the segment (Benz et al., 2004).

The supervised classification was carried out in two steps, considering first the class "Sponges" and then the other classes. The sponge backscatter areas are characterized by a roughly circular shape, a very low acoustic return and a bathymetric positive relief. Therefore, only for the class sponges, we added also the layer bathymetry to the analysis. The Template Matching (TM) algorithm was used to recognize sponge patterns. In the Template Editor, a template object was produced starting from a set of ground truth data related samples. The template is determined by means of a cross correlation layer (CCL) of the

sample characteristics in the feature space. The CCL values can range from -1 to 1, where 1 means that the template is 100% representative of the class under investigation.

To classify the remaining objects, we investigated many supervised classifiers available in eCognition, namely Classification and Regression Trees (CART), Support Vector Machine (SVM), Random Forest (RF), Bayes and K-Nearest Neighbour (KNN). The classifications were based on the GLCM entropy and mean backscatter values of the objects .In the statistical evaluation of the object features, GLCM entropy and mean backscatter gave the best class separation. The best classification results were obtained with the KNN classifier. This technique assigns the object to a certain class when the majority of the K closest samples belong to that class (Bremner et al, 2005). The value giving the best results for the classification was $K = 1$.

2.2.2 Ground truth data

The ground truth dataset comprised (i) sediment grab samples, (ii) underwater photography (drop-frame camera and transects) and (iii) underwater video transects collected within three 400 m² quadrats (Fig.2) for a total of 124 samples (Tab.2). Sampled point locations were strategically selected to include all the characteristic textural patterns identified from the backscatter imagery. We consider our samples to be representative of the various backscatter intensities, given the local consistency of the patterns targeted. The data were acquired at slack water to reduce positioning errors. The samples point locations were mapped with different buffers according to their method of acquisition. We estimated DGPS positioning errors of 0.5 m for the samples extracted from the underwater video transects, and 1 m for the sediment grabs and underwater photography (drop-frame camera and transects)

2.2.2.1 Grab samples

Ten sediment samples were collected with a Van Veen Grab (7L). The fine fraction (< 2 mm) was measured on a subsample of the top 5 cm by laser diffraction analysis (LISST 100X). Sediments were classified according to Wentworth (1922). The coarse (> 2 mm) fraction is mainly composed of fragmented shells. This bioclastic component was classified according to a semi-quantitative scale, which includes: no shell detritus, fine (and sparse) shell detritus, coarse (and dense) shell detritus. Sparse and dense refer to the detritus' spatial arrangement. Fine shell detritus is mostly composed of the shells of the Gastropod *Bittium* sp., whereas coarser detritus typically includes whole and fragmented valves, including large (> 10 cm in

9

length) dead oyster shells of *Crassostrea gigas* (Thunberg, 1793), with some degree of cementation. These samples are reported in Fig. 2 (coloured triangles).

2.2.2.2 Underwater imagery

The photographic surveys were performed on 22/11/2013 and 10/12/2013, around neap tides and slack water. Two 10-m transects were positioned over the study area. They were arranged roughly along the direction of the current, over a range of depths (from 6 m to 1.7 m). Coordinates of the transect extremities were measured with a DGPS. Pictures of 25 cm × 20 cm photoquadrats were collected (moving upstream) every 5 m on both sides of the transects, by professional technical divers (*State Police Divers, Venice Unit*).

A Go-Pro (HERO-3) camera was installed on an aluminum frame allowing operating on board by dropping the tool from the boat (drop-frame camera). Seven photoquadrats (25 cm × 20 cm) were collected over a range of bathymetries on 22 and 23/07/2014. Underwater videos were acquired using a free diver-operated Go-Pro (HERO-3) camera on 22/07/2014 over 3 areas of 20 m × 20 m (see Fig. 2), following five parallel transects in the north-south direction (diving site). A transect line was positioned straight on the seabed along the north-south axis to be followed by the diver. Initial and final transect coordinates were acquired with the DGPS system. We extracted and classified images out of the video transects, one for each meter of the line. Underwater imagery deemed unsuitable, mainly owing to water turbidity, was discarded.

2.3 Evaluation of selected mapping method

We estimated the accuracies of the models investigated by means of the confusion or error matrix, widely promoted and used in remote sensing literature (Foody, 2002). This matrix describes the pattern of class allocation made relative to the ground truth reference data, by cross-tabulating them with the predicted seafloor cover maps. To estimate the accuracies of the models we accounted on a total 100 samples excluding the 24 samples selected to train the supervised classifications (OBIA and MLC) (Table 2). For the TexAn analysis, 5 training zones were extracted within the 24 training samples from the locations of 5 drop-frames. We computed Overall, User and Producer accuracies from the raw contingency matrices. User Accuracy provides an estimate of the probability that a pixel belonging to a certain class in the classified map is that class in the real world. The Producer Accuracy is the probability that a certain seafloor class is classified as such. The Overall Accuracy provides a global estimate of how well a classifier performed, since it is the percentage of cases correctly

allocated. Moreover we calculated the Cohen s kappa coefficient (Foody, 2002). Despite manual segmentation remains amongst the most commonly used, we avoided its accuracy assessment as we retained it to be overly subjective.

3. Results

3.1 Seabed composition classes

Using 0.05-m and 0.20-m MBES grids, we observed very-fine scale heterogeneity, also reflected in the ground truth data (Table 1 and Fig. 2). The resolution used in this study allows us to observe patterns at different scales and hierarchical levels. We define five seabed classes in terms of main substrate features and habitat forming biota. These classes are distributed in patches of different size (down to less than 1 m^2).

The following classes of subtidal seabed were identified:

1) 'Sponges': massive, cushion-shaped demosponges together with associated macroalgal canopy (mainly Rodophyta and Phaeophyceae) on a bed of dead oysters of the non-indigenous species *Crassostrea gigas* (Thunberg, 1973); in Table 1 and Fig. 3, it is represented in red.

2) 'Fine shell detritus': patches of fine and sparse shell detritus (mostly the gastropod Bittium sp.) with abundant filter-feeders infauna, including Sabellidae polychaetes; in Table 1 and in Fig. 2, it is represented in grey.

3) 'Coarse shell detritus': patches of coarse and dense shell detritus (mostly whole or fragmented bivalve shells) with some degree of cementation and intensely colonised by both infauna and epifauna, mostly suspension- and filter-feeders, such as Sabellidae and Terebellidae polychaetes, anemones, ascidians; in Table 1 and in Fig. 3, it is represented in blue.

4) 'Submerged Aquatic Vegetation (SAV)': the class includes macroalgae and algal turfs on fine sediments, as well as canopy-forming macroalgae (mainly Rodophyta and Phaeophyceae) on dead oyster beds and cemented coarse shell detritus; the physical proximity between sponges and algal canopy causes a relatively noisy classification of sponges in the pixel-based methods; in Table 1 and in Fig. 3, it is represented in green.

5) 'Bare muddy bottom': patches of bare mud and sandy mud with benthic diatom film (BDF) and burrows of the thalassinid decapod *Upogebia* sp.; in Table 1 and Fig. 3, it is represented in black.

6) 'MBES artefacts': they represent the nadir artefact and artefacts due to the presence of bubbles under the transducers and to multiple reflections at the channel banks.

3.2 Mosaic Segmentation results

3.2.1 Manual segmentation

The manual segmentation identified 6 classes at both resolutions (Fig. 4b): three large-scale spatially (relatively) homogeneous 'acoustic macro-regions' and three fine-scale acoustic object classes. At the large scale we found a class identifying the detritic bottom (coarse and fine) (in turquoise in Fig. 4b); a class corresponding to bare muddy sediments (in black in Fig 4b); a class describing the patches of SAV distributed across the channel`s branches and in the SW bend (in green in Fig 4b and 4b1). At the fine scale, we detected sponges (in red in Fig. 4b and 4b1), patches of SAV and patches of detritic bottom. Two unclassified patterns were also discriminated. Draping the backscatter over the bathymetry reveals that these are ripple-like isotropic features.

3.2.2 Texture analyses with TexAn

Entropy and homogeneity were calculated for the 6 distinctive acoustic signatures identified in Table 1, used as training zones. For the 0.05-m resolution mosaic, optimal separation was achieved for *NG* = 64 grey levels, *WD* = 80 pixels, *SZ* = 50 pixels (Fig. 3, left). There is very good separation between training zones. This means the acoustic textures are best distinguished for areas 4 meters across, looking at variations over 2.5 meters approximately, and with backscatter variations with a 0.5-dB intervals (as the full backscatter range of 35 dB is divided into 64 levels). Conversely, for the 0.20-m resolution mosaic, optimal separation was achieved for *NG* = 256 grey levels, *WD* = 40 pixels, *D* = 5 pixels (Fig. 3 right). Similarly, the separation between training zones is very good. This means the acoustic textures are best distinguished for areas 8 m across looking at variations over 1 m approximately with backscatter variations within a 0.13-dB range

The class 'bare muddy bottom' (in black) has relatively less texture than the others, and it shows medium entropy and homogeneity, well clustered. It is distinct from but relatively close to the class 'coarse shell detritus' (in blue), which shows slightly higher entropy (i.e. slightly higher roughness) and slightly higher homogeneity (i.e. slightly lower textural organization, due to the presence of the coarse shells whose acoustic returns 'degrade' the underlying pattern). The class 'fine shell detritus', logically shows higher textural roughness (i.e. higher entropy) and higher homogeneity (i.e. lower textural organization again, as the textures are broken up by the small shells or, rather, the slight increases in acoustic reflectivity that they bring, depending on shell density within each pixel). All three classes

are very well constrained in terms of entropy and homogeneity, with little intra-class variation. The SAV class shows more variation in both entropy and (mostly) homogeneity. The 'sponge' class again logically shows higher entropy and a higher homogeneity (lower textural organization, corresponding to the presence of the very small structures breaking up the overall organization of the general textures. Finally, the class 'MBES artifacts' shows high homogeneities, associated to the breakdown of organization within the image, and entropies spanning the range of the other classes, in line with previous TexAn studies.

3.2.2.1 MLC with TexAn-grids

Including entropy and homogeneity layers to the MLC allows the following observations: Five classes were discriminated at 0.20-m resolution (omitting the sponge class) whereas at 0.05-m, 6 classes were mapped. At 0.20-m resolution, only the class coarse shell detritus (in Blue in Fig. 4F) appears to be coherent with the other classification methods. The remaining classes are strongly influenced by nadir artefacts and misclassification occurs almost at all places. Fine shell detritus (in Grey) covers most of the study extent, even in places where the backscatter return clearly suggests the presence of fine and unconsolidated sediments (i.e. very low backscatter). In this analysis, MBES artefacts were underestimated for the 0.20-m grids whereas using 0.05-m they were misclassified.

The method was not able to adequately separate the bare bottom classes (Grey, Blue and Black), nor to map the SAV class adequately. At 0.05-m resolution, sponges have been mapped in part. However, it is difficult to observe any coherence between their thematic appearance and the original backscatter datum. This may result from the windowing procedure (see the Discussion).

3.2.3 Jenks clustering with vectorization

The Jenks clustering procedure combined with vectorization strategies identified 6 classes at both resolutions (Fig. 4c). Noticeably, the distribution of the SAV and detritic bottom (including coarse and fine shell detritus) classes follows a similar pattern to the manual delineation. A major difference compared to the latter is the separation of coarse and fine shell detritus with Jenks' method. Spatial units representative of bare muddy bottoms are distributed accordingly but their patchiness is better captured. To a degree, the distribution of sponges is also consistent with the manual delineation; with differences evident in the SW bend of the channel. This procedure also identified MBES artifacts as an individual cluster, allowing us to map their occurrence and discard them from any habitat interpretation.

3.2.4 MLC classification

The MLC classification separated 6 classes at both resolutions. We observed the strongest coherence with the other methods in the distribution of bare muddy bottoms and coarse shell detritus (black and blue classes in figure 4d, 4d1 and Table 1). Using the 0.2-m grid, SAV patches appear significantly larger than with the other methods, covering a large part of the main body of the channel as well as the northern branches. At 0.05-m resolution, sponges are neatly mapped in the branches. However, there appears to be a strong misallocation of other features in the study area resulting in the misclassification of MBES artifacts into sponges and of detritic bottoms into SAV.

3.2.5 OBIA analysis with eCognition

The OBIA analysis using the TM and KNN algorithms identified 5 classes. The TM classification confidently identified the distribution of the sponge class (in red Fig 4E and 4E1). For the 0.05-m dataset, the created template matched 223 objects with a CCL value of 0.69. For the 0.20-m dataset, the algorithm matched 149 image objects with a CCL value of 0.78. The remaining classes, mapped by the KNN, are particularly similar to the manual segmentation.

3.2.6 Validation of segmentation methods

We estimated the Overall accuracies for all methods for the five thematic classes considered so far, for four thematic classes (obtained putting together Sponges and SAV) and for three thematic classes (obtained putting together Sponges and SAV and Fine detritus and Coarse detritus) (Fig.5 and Table A1, A2, A3 of the Appendix where also the raw confusion matrices are reported). This estimate allowed us not only to assess which classification method performed better, but also to understand the impact of the classes' choice on the accuracy and the way a habitat is ultimately thematically represented.

Overall, the pixel based methods (Jenks and MLC) performed better (even with a larger number of classes), while the texture and object based methods (OBIA, TexAn) provided significantly better accuracies when we group the classes together (Fig. 5).

The Jenks classification gave the best results in terms of Overall accuracy, varying in the different cases from 0.6 for the 0.2-m grid and five classes to 0.83 for the 0.05-m grid and three classes. Similarly the kappa values varied from 0.5 to 0.72. Only for the case of the 0.05-m grid and four classes, the MLC classification performed slightly better than Jenks.

On the other hand OBIA analyses had an overall agreement ranging from 0.51 in the case of the 0.2-m grid and five classes up to 0.66 for 0.05-m grid and three classes. The kappa coefficient for OBIA was quite stable varying from 0.38 to 0.46. Concerning TexAn, the Overall accuracy and the kappa coefficient were similar to what would be expected by chance for five classes, while it improved for three classes (Figure 5).

Overall we obtain better accuracies for the 0.05-m resolution compared to the 0.20-m resolution. This may be due to the fact that the 0.05 grid represents better the continuous variations in the seafloor surface and the indeterminate boundaries among classes, that are lost through the 'hard' classification (Lucieer and Lucieer, 2009, Foody, 2002). Moreover if the 0.20m pixels represent areas containing more than one class, the mixed pixels could be an important cause of misclassification, particularly where the seafloor mosaic is complex and heterogeneous (Foody, 2002). In all cases, accuracies and kappa coefficients increased as the number of classes decreased. For further analysis of the accuracy assessment User and Producer accuracy estimates are reported in the Appendix

4. Discussion

4.1 Relative success of segmentation methods

Recent publications proposed comparative approaches to the segmentation of MBES products (e.g. Diesing et al. 2014 and Calvert et al. 2014). In this work, we investigated the potential application of very high resolution backscatter segmentation in extremely shallow areas, seldom explored with acoustic methods. Through MBES data and geo-referenced seabed imagery, we characterised an extremely shallow benthic environment.

Ferrini and Flood (2006) suggested that backscatter intensity alone cannot be used to quantitatively predict seabed characteristics. Other studies carried out in Australia (e.g. Ierodiaconou et al. 2011; Lucieer et al., 2013) needed to analyze backscatter as well as bathymetry to improve the classification of the benthic substrata. In our study, the use of bathymetry is not strictly necessary since: a) the substrate is not only bare sandy sediment as in Ferrini and Flood (2006) and b) the resolution of the backscatter was such that we could identify the characteristic acoustic signature of single biogenic features (like individual sponges, or clumps depending on the nature of the method) and map their distribution throughout the study area.

The Lagoon of Venice presents high heterogeneity at different scales and complex horizontal and vertical environmental gradients (Sigovini, 2011; Tagliapietra et al., 2009). Lagoon

bottom is known to be characterized by large and fine scale gradients as well as a mosaic of morphologies and habitats with a patchy distribution (Garcıa-Charton and Pe`rez-Ruzafa, 1998 and 2000; Perez-Ruzafa et al. 2007). Habitat margins (or 'borders' between units/patches) are often vaguely defined. This feature calls for the application of segmentation methods which depict this textural intricacy (Fortin et al, 1995; Fortin et al. 2000). In this regard, we have seen that manual segmentation can detect fine-scale biotic features and discriminate seafloor macro-regions. However, when the user exercises digitization over a broad study extent, subtle grey-level variations remain easily undetected. For example, in our case, the manual segmentation failed to distinguish among fine and coarse mixed bioclastic detritus. When the resolution of the analysis is enhanced, it is easier for the observer to discriminate seafloor features down to single objects. For example, with the manual segmentation, it was possible to map the sponge distribution. This requires a two-phase digitization approach, though, in which objects with different size are mapped in steps. This is time-consuming, non-repeatable, imprecise and strongly dependent upon user expertise and the extent of the observation (Micallef et al., 2012, Diesing et al., 2014).

Similarly, we argue that TexAn may produce more reliable results with coarser data resolutions and in larger-scale studies (Huvenne et al. 2002 and 2007). Computation windows need to be large enough to encompass textural variations of interest, and small enough that do not mix different textural signatures. For the 0.20-m grid, best results were obtained for areas 8 m across (respectively 4 m for the 0.05-m resolution dataset). Textural variations were best distinguished over scales of 1 m approximately (respectively 2.5 m). Whereas TexAn could adequately cope with the high backscatter resolution (0.13-dB per grey level), this method extracted information of different nature compared to the clustering-based methods. TexAn identified areas in which sponges occur, rather than mapping out individual sponges or clumps. This averages out a significant amount of data points given the fine resolution of the data herein used, resulting in the mapping of relatively large areas. Textural analysis was also strongly influenced by nadir linear artifacts due to their highly homogeneous signature. Coverage of a large area of extremely shallow seafloor requires the mosaicking of many narrow swaths, hence many nadir pixels; sonars with larger swaths (deeper water) will not encounter this problem to the same extent.

Similarly to the other methods, the pixel-based MLC segmentation was successful in discriminating classes with homogeneous grey level values (i.e. coarse shell detritus and sponges). Nonetheless, the classes with very heterogeneous backscatter were mostly (i.e.

16

SAV) confused with bare muddy bottom and sponges due to their shared spectral attributes. As an attempt to improve the results, the sponge class variance was reduced by digitizing irregular polygons to encompass their characteristic backscatter signature.

Moreover, combining together the class sponge and class SAV improves the classification (see Figure 5 and the raw confusion matrices in the Appendix). Investigating the effect of training sample size and shape on fine scale backscatter imagery will inevitably contribute to a more robust use of MLC classifications. However as the method assumes Gaussian distribution of the data, it may be not adequate for mapping of heterogeneous backscatter signatures as in nature normal distributions are often not the case (Reimann and Filzmoser, 2000).

Micallef et al. (2012) suggested that including textural indices in the MLC may strengthen the classification. To check this, we performed a second MLC using the TexAn results for homogeneity and entropy and applied a Principal Component Analysis (PCA) at both resolutions investigated. For the 0.05-m dataset, the PCA revealed that backscatter explains 89.2 %, homogeneity 1.3 % and entropy 9.4 % of seafloor variability. For the 0.2-m dataset, backscatter explained 52.6 %, homogeneity 0.5 % and entropy 46.8 %, respectively. As the scale increases, other variables than backscatter alone tend to become more important. This is probably because the number of backscatter outliers decreases, limiting the range of possible backscatter values and stabilising the textural indices.

With regard to the OBIA analysis, one of its major advantages is that the image is processed by taking into account collections of pixels which together constitute image objects. The objects contain more information than single pixels, having their own statistics, shape, size, relations and hierarchy. Images separated into objects better reflect the way in which the human brain recognizes patterns (e.g. Hay and Castilla, 2006) and possibly, the patchy nature and spatial configuration of various natural systems. Similarly to others (i.e. Lüdtke et al. 2012; Stephens and Diesing, 2014), we noticed that the KNN performs well when the image is preceded by small scale multiresolution segmentation. However, our investigation shows that increasing the K parameter decreased diversity of class distribution, resulting in a less accurate classification. For example, with $K = 2$, the number of classes was only 3 and from $K = 5$, only two classes were mapped.   The TM was useful at mapping sponges showing promising results in a context of seabed monitoring and automatization of classification routines in habitat mapping studies. In our case in many places high values of CCL matched segments that were in neighbourhood or near to the border of the real sponges segments. In

this method however, the poor accuracy obtained for the sponges may be related to the template quality which is affected by complex parameters, like ground truth tolerance, size and others. The template was also designed more on the largest ground truth sponges and the latter did not overlap with the smaller ground truth transects within the diving site. There are many ways to improve the TM processing, like creating few sizes of very high quality templates or connecting the TM with suitable features of OBIA segments, like elliptic fit or specified for sponges range of mean backscatter intensity. Nonetheless, it is important to underline that for the sponge class in this analysis, the CCL value represents an accuracy metric of its own as it expresses the degree to which sponge templates have been correctly matched. Clearly, positional accuracy of very small scale features hinders the statistical accuracy assessment by means of confusion matrices.

Jenks' clustering method combined with vectorization produced good results for our study area. For the most part, the predicted distribution of habitats is consistent with the ground truth data. Goodness of Variance Fit proved to be a valuable index to select clustering local *optima*. Including vectorization strategies, we could overcome the critical issue of seabed features looking and sounding the same. In this way, we could separate sponges from patches of unconsolidated fine sediments without any specialized data processing methods.

Yet the quantitative assessment using confusion matrices suggests that we were not able to fully calibrate the data to the ground truth information (not for all classes). This is an issue inherent to the very fine resolution of the grids herein used and calls for labour intensive and costly ground truth protocols which will be focus of our future research. Furthermore it is important to consider the temporal dynamicity of the study site which clearly represents a further source of incompatibility between ground truth and acoustic data. This is due to ecological processes (which so far remain unquantified) such as the growth or death of sponges and SAV, which can drastically modify the seascape.

Interestingly, we researched the effect of merging classes on the final accuracy estimates. Similarly to Rattray et al. (2013), we merged the sponge and SAV classes producing the equivalent of the ALG/INV class there defined as a mixed class at the interface of algal and invertebrate dominated reef habitats and recomputed the analysis over the contingency matrices for all methods. This shows that accuracies can be greatly improved, but at the cost of describing the habitat under study in more general terms, losing the possibility to map the distribution of single sponges.

18

As such, while the very high resolution backscatter allows for a full appreciation of the complexity of the system under study (its substrate composition) and conveys a great amount of information comparing to coarser resolution datasets, from the perspective of thematic classification, there is a limitation in the way the system is ultimately depicted. Thereby, there is a clear trade-off between the strength of the accuracy and the amount and type of features which are mapped. This implies that a compromise will inherently be present when seabed type and features are mapped simultaneously within the classification approach. Nonetheless, our results show that simple clustering of MBES backscatter can be a very efficient way to describe and acknowledge the investigated distribution of benthic habitats in the environmental context.

4.1 Temporal variability

The tidal channel under study is subject to dynamical processes which lead to temporal changes of the substrate. As we were not able to assess the temporal variability of the system, we consider our product to be a '*snapshot in time*' as defined in Brown et al. (2011). This observation also emphasises the importance of collecting ground truth samples complementary to the acoustic survey in comparable amounts of time (which was not always possible in our study, with some samples gathered 7 months after the survey). This is particularly true in view of habitat modifications given by seasonal environmental changes such as vegetation growth, which can drastically modify the seascape, particularly in shallow and highly productive estuaries (Valiela et al. 1997).

5. Conclusion

In this study, we present the results of benthic habitat mapping through very high-resolution MBES data and ground truth samples in an extremely shallow environment. Benthic habitat mapping in these environments, particularly in lagoons, has been rarely carried out due to a range of logistic issues. Lagoon channels present specific operational challenges of which strong currents, high turbidity and vessel traffic. Thus, up to now, these environments have been almost unexplored. Using MBES and ground-truth data, it has been possible not only to explore and map a tidal channel benthic substrate, but also to map ecologically noteworthy biogenic features such as sponges. In our study, we compared different approaches of unsupervised and supervised classification to assess the advantages and limits of each method and their efficacy in correctly identifying very fine scale features and broader classes. We discussed the relative merits of each method and particularly, discussed the issues relating to

high accuracy MBES data, ground truth positioning error and their effect on statistically derived accuracies.

The mapping of tidal environment substrata is of high relevance, also from a legal perspective, as it may form the basis of policy-making processes and the implementation of educated decisions, particularly for the designation of Marine Protected Areas (MPAs). Following on observations by Franco et al. (2006), our results show that tidal channels possess a range of habitats extremely valuable for the lagoon biodiversity (i.e. nursery grounds, bio-physical coupling, etc.). A deeper understanding of virtually unexplored habitats provides crucial information on the occurrence and distribution of ecologically important biogenic features. This assessment opens a totally new perspective in the knowledge-based management of natural resources in very shallow coastal areas.

Acknowledgments

References

Barbier, E. B., Hacker, S. D., Kennedy, C., Koch, E. W., Stier, A. C., and Silliman, B. R. 2011. The value of estuarine and coastal ecosystem services. Ecological Monographs, 81(2), 169-193.

Benz, U.C., P. Hofmann, G. Willhauck, I. Lingenfelder and Heynen, M. 2004. Multi-resolution, object-oriented fuzzy analysis of remote sensing data for GIS-ready information. ISPRS Journal of Photogrammetry & Remote Sensing, 58, 239-258.

Bivand, R., Ono, H., and Dunlap, R. 2009. classInt: choose univariate class intervals. R package version 0.1-14.

Blondel, P. 1996. Segmentation of the Mid-Atlantic Ridge south of the Azores, based on acoustic classification of TOBI data. Geological Society, London, Special Publications, 118(1), 17-28.

Blondel, P. 2009. The Handbook of Sidescan Sonar. Springer Praxis: Heidelberg, 345 pp.

Blondel, P., Gómez Sichi, O. 2009. Textural analyses of multibeam sonar imagery from Stanton Banks, Northern Ireland continental shelf. Applied Acoustics, 70(10), 1288-1297.

Blondel, P., Sempéré, J. C., and Robigou, V., 1993. Textural analysis and structure-tracking for geological mapping: applications to sonar images from Endeavour Segment, Juan de Fuca ridge. In OCEANS'93. Engineering in Harmony with Ocean. Proceedings. IEEE, (3), 209-213.

Blondel, P., Parson, L. M., and Robigou, V. 1998. TexAn: textural analysis of sidescan sonar imagery and generic seafloor characterisation. In OCEANS'98 Conference Proceedings IEEE, (1), 419-423

Blondel, P., 2000. Automatic mine detection by textural analysis of COTS sidescan sonar imagery. International Journal of Remote Sensing, 21(16), 3115-3128.

Blondel, Ph. (ed.), 2012. "Bathymetry and Its Applications", InTech, 148 , ISBN 978-953-307-959-2, (http://www.intechopen.com/books/show/title/bathymetry-and-its-applications), doi: 10.5772/2132

Bremner, D., Demaine, E., Erickson, J., Iacono, J., Langerman, S., Morin, P., Toussaint, G., 2005. Output-Sensitive Algorithms for Computing Nearest-Neighbour Decision Boundaries. Discrete and Computational Geometry 33, 593-604.

Brown, C. J., Blondel, P. 2009. Developments in the application of multibeam sonar backscatter for seafloor habitat mapping. Applied Acoustics, 70(10), 1242-1247.

Brown, C. J., Smith, S. J., Lawton, P., Anderson, J. T., 2011. Benthic habitat mapping: A review of progress towards improved understanding of the spatial ecology of the seafloor using acoustic techniques. Estuarine, Coastal and Shelf Science, 92(3), 502-520.

Calvert, J., Strong, J. A., McGonigle, C., Quinn, R., 2014. An evaluation of supervised and unsupervised classification techniques for marine benthic habitat mapping using multibeam echosounder data. ICES Journal of Marine Science: Journal du Conseil, fsu223.

CARIS 2009. CARIS HIPS and SIPS Training Manual. 14-18 September 2009.

Corriero, G., Longo, C., Mercurio, M., Marchini, A., Occhipinti-Ambrogi, A., 2007. Porifera and Bryozoa on artificial hard bottoms in the Venice Lagoon: Spatial distribution and temporal changes in the northern basin. Italian Journal of Zoology, 74(1), 21-29.

Costanza, R, D'Arge, R., Groot, R. D., Farber, S., Grasso, M., Hannon, B., Limburg, K., Naeem, S., O'Neill, R., Paruelo, R., Robert G., Sutton, P., Belt M, V., 1998. The value of the world's ecosystem services and natural capital. Nature. 387(6630), 253-260.

Dalrymple, R. W., Rhodes, R. N., 1995. Estuarine dunes and bars. Geomorphology and sedimentology of estuaries, 53, 359-422.

De Falco, G., Tonielli, R., Di Martino, G., Innangi, S., Simeone, S., and Michael Parnum, I., 2010. Relationships between multibeam backscatter, sediment grain size and Posidonia oceanica seagrass distribution. Continental Shelf Research, 30(18), 1941-1950.

Diesing, M., Green, S. L., Stephens, D., Murray Lark, R., Stewart, H. A., and Dove, D., 2014. Mapping seabed sediments: Comparison of manual, geostatistical, object-based image analysis and machine learning approaches. Continental Shelf Research. (84), 107-119.

EMODnet. (2015). EMODnet Portal for Batymethry. Available: http://www.emodnet-hydrography.eu/ . Last accessed 21th April 2015.

Erdey-Heydorn, M.D., 2008. An ArcGIS seabed characterization toolbox developed for investigating benthic habitats. Marine Geodesy, 31(4): 318-358.

ESRI 2015. ArcGIS Desktop: Release 10.2. Redlands, CA: Environmental Systems Research Institute.

Ferrini, V. L., & Flood, R. D., 2006. The effects of fine-scale surface roughness and grain size on 300 kHz multibeam backscatter intensity in sandy marine sedimentary environments. Marine Geology, 228(1), 153-172.

Fonseca, L., & Calder, B. (2005). Geocoder: an efficient backscatter map constructor. In *Proceedings of the US Hydrographic Conference*, 29-31.

Fortin, M. J., and Drapeau, P., 1995. Delineation of ecological boundaries: comparison of approaches and significance tests. Oikos, 72, 323-332.

Fortin, M. J., Olson, R. J., Ferson, S., Iverson, L., Hunsaker, C., Edwards, G., and Klemas, V., 2000. Issues related to the detection of boundaries. Landscape Ecology, 15(5), 453-466.

Foody, G. M., 2002. Status of land cover classification accuracy assessment. Remote Sensing of Environment, 80, 185-201.

Franco, A., Franzoi, P., Malavasi, S., Riccato, F., & Torricelli, P. (2006). Fish assemblages in different shallow water habitats of the Venice Lagoon. In Marine Biodiversity , 55, 159-174.

Galparsoro, I., X. Agrafojo, M. Roche, K. Degrendele. 2015. Comparison of supervised and unsupervised automatic classification methods for sediment types mapping using multibeam echosounder and grab sampling, Italian Journal of Geosciences, 1314(1), 41-49.

Gao, D., Hurst, S.D., Karson, J.A., Delaney, J.R., Spiess, F.N., 1998. Computer-aided interpretation of side-looking sonar images from the eastern intersection of the Mid-Atlantic Ridge with the Kane Transform. Journal of Geophysical Research, 103, 20997-21014

Garcıa-Charton, J.A., Pérez-Ruzafa, A., 1998. Correlation between habitat structure and a rocky reef fish assemblage in the southwest Mediterranean. PSZN Marine Ecology 19, 11-128.

Garcıa-Charton, J.A., Williams, I.D., Pérez-Ruzafa, A., Milazzo, M.,Chemello, R., Marcos, C., Kitsos, M.S., Kokouras, A., Riggio, S., 2000. Evaluating the ecological effects of Mediterranean marine protected areas: habitat, scale and the natural variability of ecosystems. Environmental Conservation 27, 159 -178.

Guelorget, O., and Perthuisot, J. P., 1992. Paralic ecosystems. Biological organization and functionning. Vie et milieu, 42(2), 215-251.

Halpern, B. S., Walbridge, S., Selkoe, K. A., Kappel, C. V., Micheli, F., D'Agrosa, C., Watson, R., 2008. A global map of human impact on marine ecosystems. Science, 319 (5865), 948-952.

Hay, G. J., and Castilla, G. 2006. Object-based image analysis: strengths, weaknesses, opportunities and threats (SWOT). International Archives of Photogrammetry, Remote Sensing and Spatial Information Sciences, 36(4), 1-3.

Hijmans, R. J., van Etten, J., Mattiuzzi, M., Sumner, M., Greenberg, J. A., Lamigueiro, O. P., and Hijmans, M. R. J., 2014. Package 'raster'.

Huvenne, V. A., Hühnerbach, V., Blondel, P., Gómez Sichi, O., and LeBas, T., 2007. Detailed mapping of shallow-water environments using image texture analysis on sidescan sonar and multibeam backscatter imagery. In 2nd International Conference & Exhibition on "Underwater Acoustic Measurements: Technologies & Results", 879-886.

Huvenne, V. A. I., Blondel, P., & Henriet, J. P. (2002). Textural analyses of sidescan sonar imagery from two mound provinces in the Porcupine Seabight.*Marine Geology*, *189*(3), 323-341.

Ierodiaconou, D., Laurenson, L., Burq, S., and Reston, M., 2007. Marine benthic habitat mapping using Multibeam data, georeferencedvideo and image classification techniques in Victoria, Australia. Journal of Spatial Science, 52(1), 93-104.

Ierodiaconou, D., Monk, J., Rattray, A., Laurenson, L., and Versace, V. L., 2011. Comparison of automated classification techniques for predicting benthic biological communities using hydroacoustics and video observations. Continental Shelf Research, 31(2), S28-S38.

Kennish, M. J., 2002. Environmental threats and environmental future of estuaries. Environmental conservation, 29(1), 78-107.

Kenny, A. J., Cato, I., Desprez, M., Fader, G., Schüttenhelm, R. T. E., and Side, J., 2003. An overview of seabed-mapping technologies in the context of marine habitat classification. ICES Journal of Marine Science: Journal du Conseil, 60(2), 411-418.

Kirwan, M. L., and Megonigal, J. P., 2013. Tidal wetland stability in the face of human impacts and sea-level rise. Nature, 504(7478), 53-60.

Lu, D., and Weng, Q. 2007. A survey of image classification methods and techniques for improving classification performance. International journal of Remote sensing, 28(5), 823-870.

Lucieer, V., and Lucieer, A. 2009. Fuzzy clustering for seafloor classification. Marine Geology, 264(3), 230-241.

Lucieer, V., Hill, N. A., Barrett, N. S., and Nichol, S., 2013. Do marine substrates 'look'and 'sound' the same? Supervised classification of multibeam acoustic data using autonomous underwater vehicle images. Estuarine, Coastal and Shelf Science, 117, 94-106.

Lucieer, V., Lamarche, G., 2011. Unsupervised fuzzy classification and object-based image analysis of multibeam data to map deep water substrates, Cook Strait, New Zealand. Continental Shelf Research 31, 1236–1247.

Lüdtke, A., Jerosch, K., Herzog, O., and Schlüter, M., 2012. Development of a machine learning technique for automatic analysis of seafloor image data: Case example, Pogonophora coverage at mud volcanoes. Computers & Geosciences, 39, 120-128.

Lundblad, E., Wright, D.J., Miller, J., Larkin, E.M.,Rinehart, R., Battista,

T., Anderson, S.M., Naar, D.F., and Donahue, B.T., 2006. A benthic terrain

classification scheme for American Samoa, Marine Geodesy, 29(2): 89-111.

Maggiore F., Keppel E., 2007, Biodiversity and distribution of polychaetes and molluscs along the Dese estuary (Lagoon of Venice, Italy). Hydrobiologia, 588(1): 189-203.

McBreen, F., Askew, N., Cameron, A., Connor, D., Ellwood, H., Carter, A., 2011. UK SeaMap 2010 Predictive mapping of seabed habitats in UK waters, JNCC Report 446, ISBN 0963 8091. 103pp. Available online at http://jncc.defra.gov.uk/PDF/jncc446_web.pdf.

McGlathery, K. J., Sundback, K., and Anderson, I. C., 2007. Eutrophication in shallow coastal bays and lagoons: the role of plants in the coastal filter. Marine Ecology Progress Series, 348, 1-18.

McGonigle, C., Collier, J., 2014. Interlinking backscatter, grain size and benthic community structure. Estuarine, Coastal Shelf Science 147, 123-136.

MESH, 2008. MESH Confidence Assessment. Available online at http://www.searchmesh.net/default.aspx?page=1635 .

Micallef, A., Le Bas, T. P., Huvenne, V. A., Blondel, P., Hühnerbach, V., and Deidun, A., 2012. A multi-method approach for benthic habitat mapping of shallow coastal areas with high-resolution multibeam data. Continental Shelf Research, 39, 14-26.

NOAA., 2014. How much of the ocean have we explored? http://oceanservice.noaa.gov/facts/exploration.html.

Occhipinti Ambrogi A., Gola G., 2001. Macrozoobenthos di fondo incoerente in Laguna di Venezia: contributo alla conoscenza del bacino di Malamocco. Biol. Mar. Mediterr., 8 (1), 393-402.

Parnum, I. M., Gavrilov, A. N., 2011. High-frequency multibeam echo-sounder measurements of seafloor backscatter in shallow water: Part 1 - Data acquisition and processing. Underwater Technology 30 (1), 3-12.

Pranovi F., Curiel D., Rismondo A., Marzocchi M., Scattolin M., 2000. Variation of the macrobenthic community in a seagrass transplanted area of the lagoon of Venice. Sci. Mar., 64(3): 303-310.

R Core Team., 2014. R: A language and environment for statistical computing. R Foundation for Statistical Computing, Vienna, Austria. URL http://www.R-project.org/.

Reimann, C., & Filzmoser, P. (2000). Normal and lognormal data distribution in geochemistry: death of a myth. Consequences for the statistical treatment of geochemical and environmental data. *Environmental geology*, *39*(9), 1001-1014.

Seo, B., Bogner, C., Poppenborg, P., Martin, E., Hoffmeister, M., Jun, M., Koellner, T., Reineking, B., Shope, C. L., and Tenhunen, J. (2014). Deriving a per-field land use and land cover map in an agricultural mosaic catchment. Earth System Science Data, 6(2), 339-352.

Sfriso A., Birkemeyer T., Ghetti P.F., 2001. Benthic macrofauna changes in areas of Venice lagoon populated by seagrasses or seaweeds. Marine Environmental Research, 52: 323-349.

Sigovini, M., 2011. Multiscale dynamics of zoobenthic communities and relationships with environmental factors in the lagoon of Venice. PhD thesis, Università Ca' Foscari Venezia, 207.

Sigovini M., Foglini F., Keppel E., Kruss A., Manfrin F., Tagliapietra D., Zaggia L., Madricardo F., 2014. Habitat mapping in coastal lagoons: first results on a tidal channel and future prospects. Biologia Marina Mediterranea 20 (1).

Solidoro, C., Bandelj, V., Bernardi, F. A., Camatti, E., Ciavatta, S., Cossarini, G., and Torricelli, P. 2010. Response of the Venice Lagoon Ecosystem to Natural and Anthropogenic Pressures over the Last 50 Years. From: Coastal Lagoons: Critical Habitats of Environmental Change, (19) 483-511.

Stephens D, Diesing M, 2014. A Comparison of Supervised Classification Methods for the Prediction of Substrate Type Using Multibeam Acoustic and Legacy Grain-Size Data. PLoS ONE 9(4), e93950.

Tagliapietra D, Sigovini M, Volpi Ghirardini A, 2009, A review of terms and definitions to categorise estuaries, lagoons and associated environments. Marine and Freshwater Research 60 (6), 497-509.

Tagliapietra D., Pavan M., Wagner C., 1998. Macrobenthic community changes related to eutrophication in Palude della Rosa (Venetian lagoon, Italy). Estuarine Coast and Shelf Science, 47 (2): 217-226.

Udvardy, M.F.D., 1959. Notes on the ecological concepts of habitat, biotope and niche. Ecology, 40, 725–728.

Umgiesser, G., Canu, D. M., Cucco, A., and Solidoro, C. (2004). A finite element model for the Venice Lagoon. Development, set up, calibration and validation. Journal of Marine Systems, 51(1), 123-145.

Valiela, I., McClelland, J., Hauxwell, J., Behr, P. J., Hersh, D., and Foreman, K., 1997. Macroalgal blooms in shallow estuaries: controls and ecophysiological and ecosystem consequences. Limnology and Oceanography, 42(5part2), 1105-1118.

Vatova A., 1940. Le zoocenosi della Laguna veneta. Thalassia, 3(10): 1-28.

Wang, C. K., and Philpot, W. D., 2007. Using airborne bathymetric lidar to detect bottom type variation in shallow waters. Remote Sensing of Environment,106(1), 123-135.

Wentworth, C. K., 1922. A scale of grade and class terms for clastic sediments. The Journal of Geology, 377-392.

Wright, D. J., Lundblad, E. R., Larkin, E. M., Rinehart, R. W., Murphy, J., Cary-Kothera, L., and Draganov, K., 2005. ArcGIS benthic terrain modeler. Oregon State University, Corvallis, OR, USA.

Figure captions
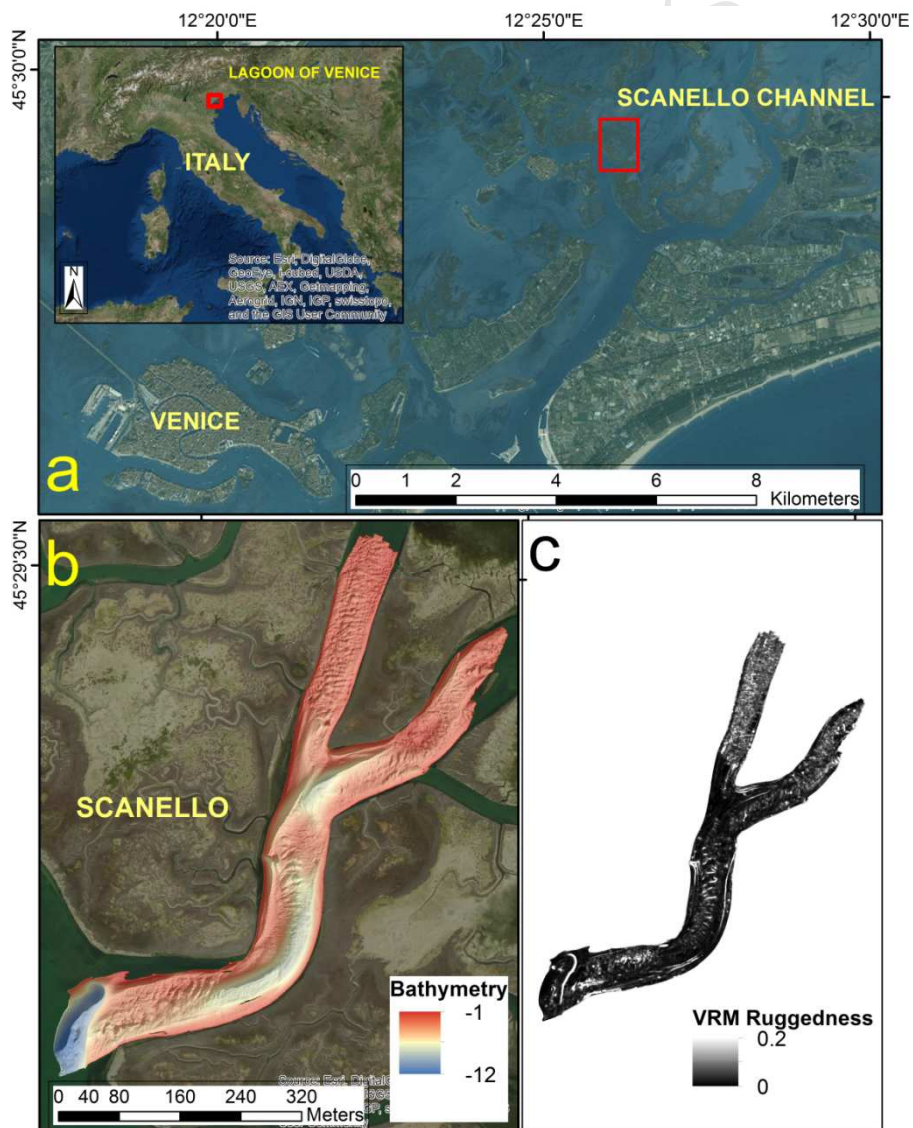
Figure 1 - Geographical setting: a) The Lagoon of Venice; (ESRI LPK aerial satellite imagery at 30 cm resolution, with inset general setting); b) Shaded bathymetry of the Scanello channel (DTM resolution 0.05 m, 5 times vertical exaggeration), set against a synoptic satellite image of its immediate surroundings. The satellite image is dated 25th November 2013.); c) Vector ruggedness measure (VRM) calculated over a 5×5 neighborhood (Benthic Terrain Modeler, Wright et al. 2005).
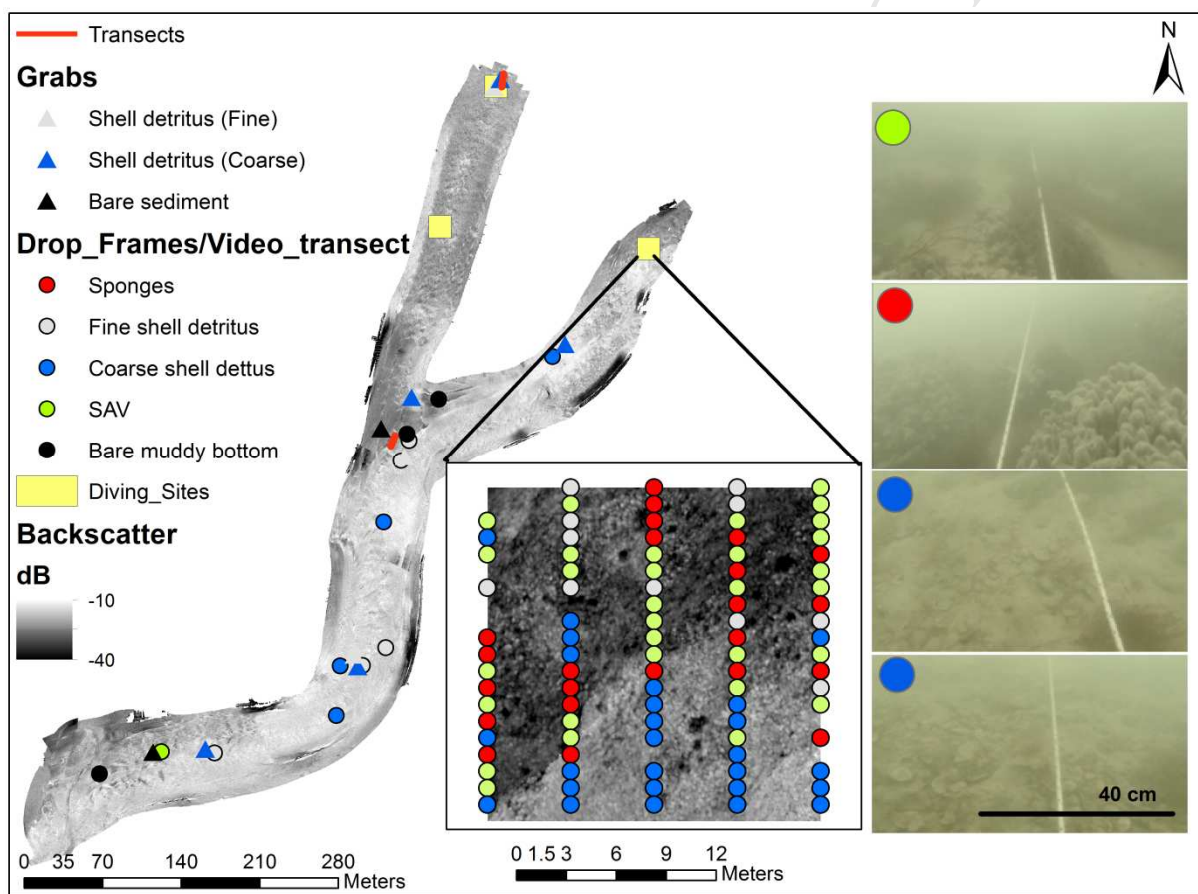
Figure 2 - *Left:* Backscatter map of the study area, with the locations of drop frames, three diving sites, grab samples and photo-transects. Black, Grey and Blue triangles show the locations of grab samples. *Center*: close-up view of the backscatter at diving site 3, with the location of the images extracted from the video transects. *Right*: examples of video transect image. The colour of the circle in the photographs represents the corresponding class.
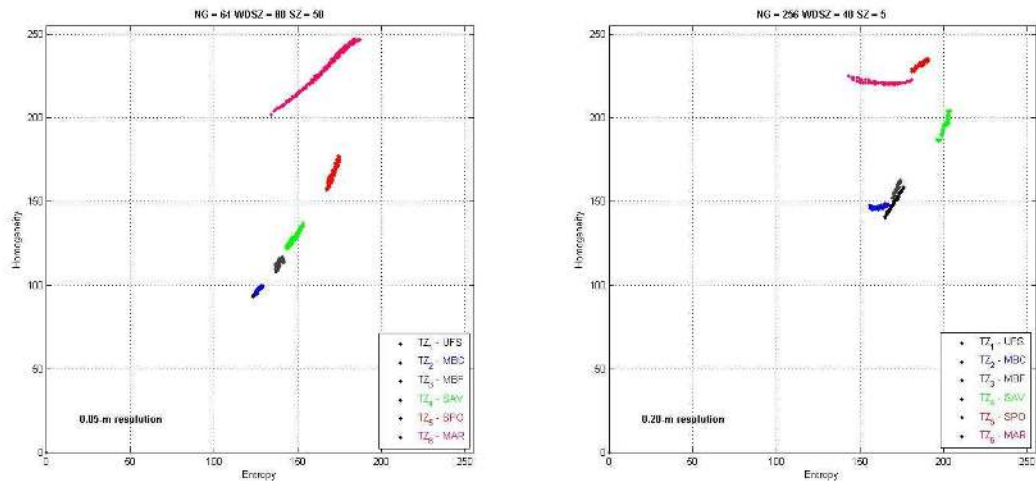
Figure 3 – Textural separation between the 6 distinct acoustic signatures identified in Table 1, for the 0.05-m resolution mosaic (left) and the 0.20-m resolution mosaic (right). See text for details.
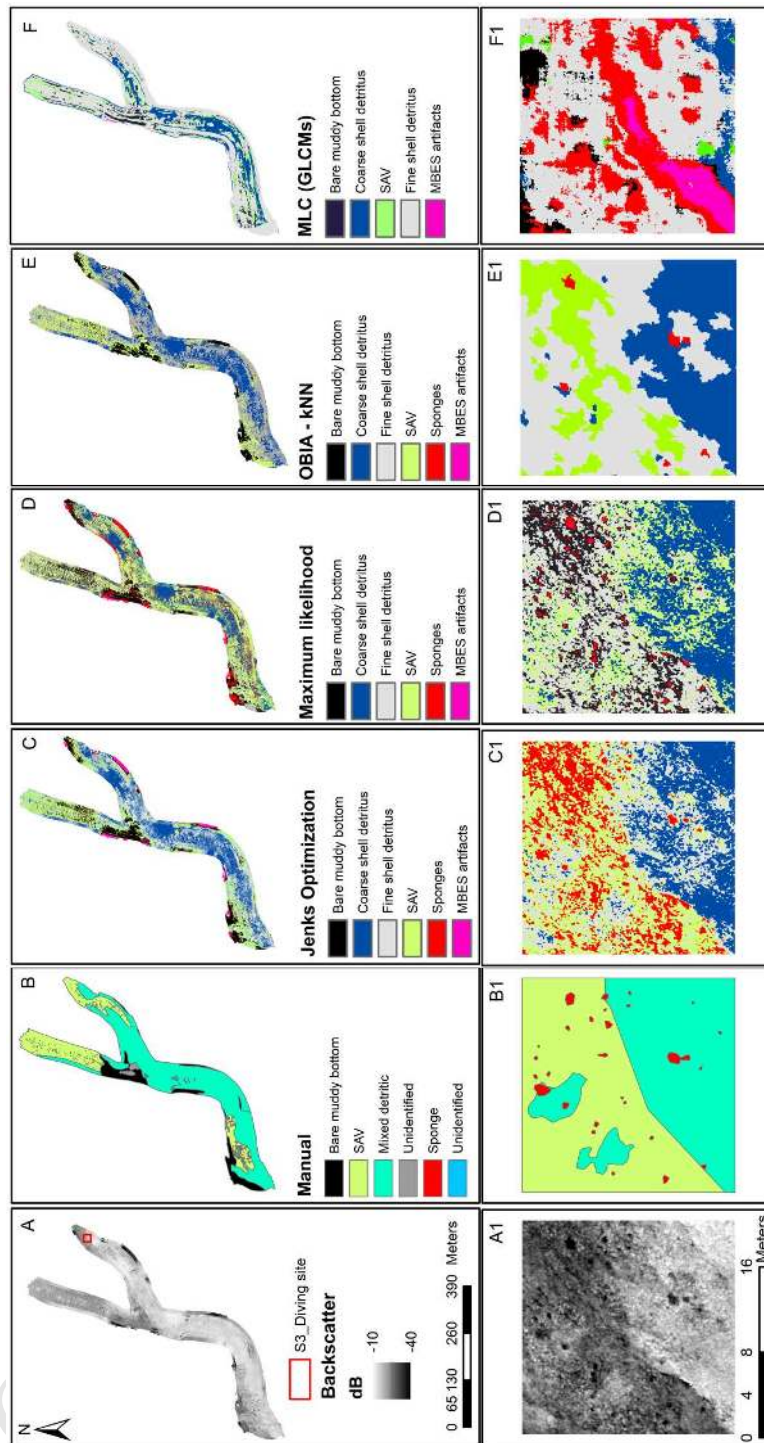
Figure 4 – Top row: Backscatter data and classification results with the different methods using the 0.2-m grid. Bottom row: 20 m × 20 m spatial unit backscatter and segmentations at 0.05-m resolution. Refer to text and Table 1 for explanation of abbreviations and classes.

31
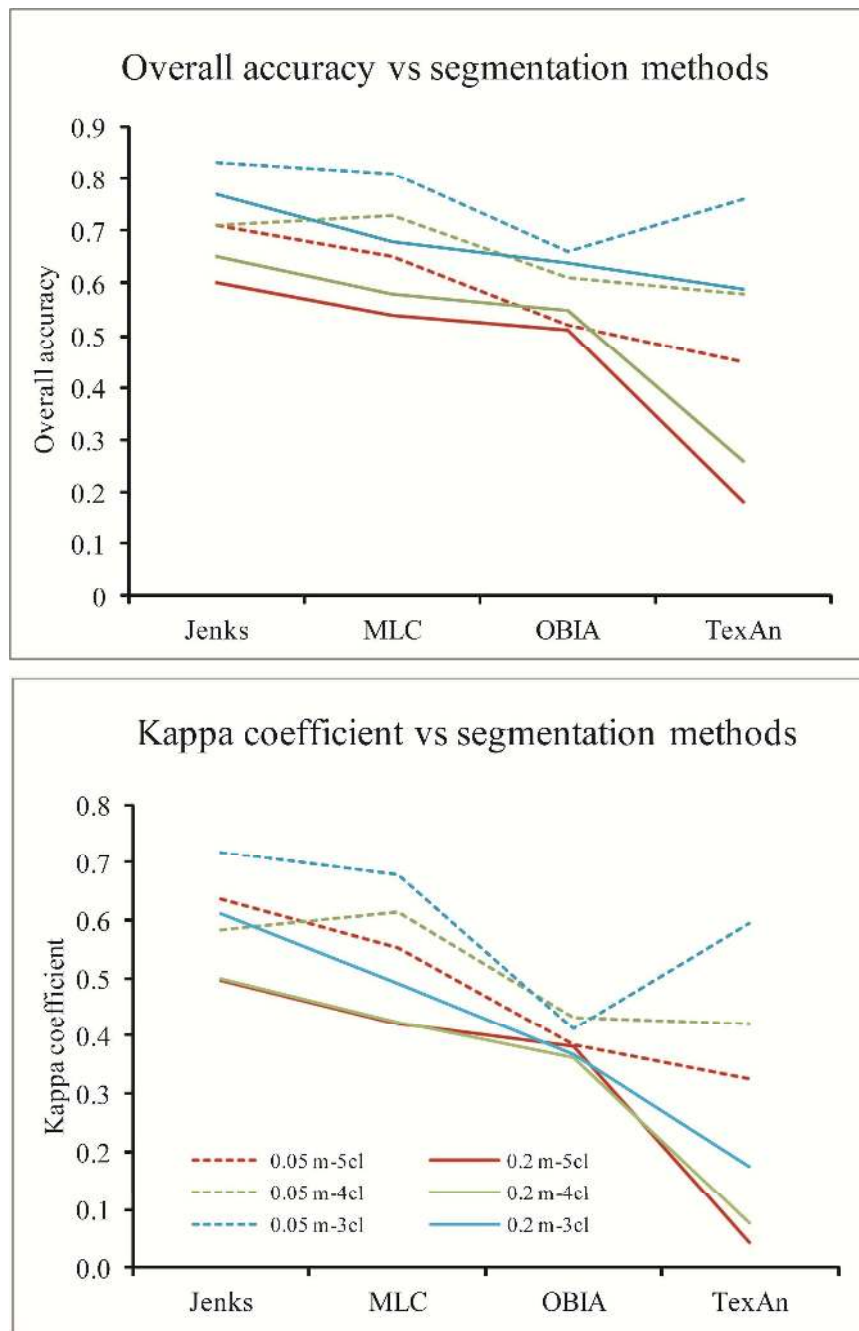
Figure 5. Overall accuracy and kappa coefficient for each segmentation method ant its

dependence on the number of classes: the *red* colour represents the 5 classes (sponges, fine

detritus, coarse detritus, SAV and bare mud), *green* the 4 classes (sponges+SAV, fine

detritus, coarse detritus and bare mud), *blue* the 3 classes (sponges+ SAV, fine + coarse

detritus, bare mud) segmentations. Solid and dashed lines represent the 0.2 m and 0.05 m grid

resolution, respectively. Values are reported in Table A1, A2 and A3 of the appendix.

Table captions

Table 1 - Distinctive backscatter signatures present within the study area and correspondent

classes and ground-truth images.
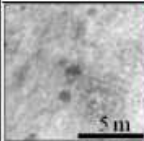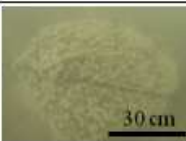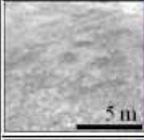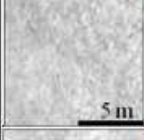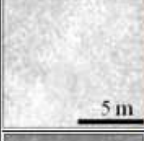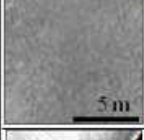
Backscatter Image	Class colour\ID	Texture description	Seabed image	Seabed composition	Sample ID
	1	Low backscatter signature described by circular shapes		Massive demosponges and macroalgal canopy on a bed of dead oysters Crassostrea gigas (Thunberg, 1973)	Diving site S2
	2	Wave-like pattern of low backscatter signatures		Macroalgae and algal turfs on fine sediments and canopy-forming macroalgae on dead oyster bed	Drop-frame V7
	3	Speckled pattern of high backscatter signature		Patches of fine and sparse shell detritus (mostly Bittium sp.) with Sabellidae	Drop-frame V1
	4	Speckled pattern of high homogenoeus backscatter		Patches of coarse and dense shell detritus (mostly bivalves) with some degree of cementation and colonised by both infauna and epifauna	Drop-frame V4
	5	Low backscatter signature composing large patches		Patches of bare mud and sandy mud with benthic diatom film and Upogebia burrows	Drop-frame V6
	6	Very low homogenous backscatter signature	na	Multi-beam echosounder navigation artifacts	na

Table 2 – *Summary of the type of samples, their number and how the used in this study*

sample type/use	grabs	video-transects	photo-transects	drop-frames	total
training	4	14	0	6	24
accuracy	6	77	10	7	100
total	10	91	10	13	124

Appendix 1 - Accuracy assessment

Table A1. User, Producer and Overall accuracies for the different classification methods into five classes for the 0.05 m and 0.2m grid resolution

Method	Class/Accuracy	005 m Grids				02 m Grids			
		Producer	User	Overall	kappa	Producer	User	Overall	kappa
Jenks	Sponges	0.9	0.82			0.93	0.6		
	Fine Det.	0.46	0.84			0.24	0.5		
	Coarse Det.	0.9	0.57	0.71	0.63	0.95	0.57	0.6	0.49
	SAV	0.87	0.76			0.58	0.64		
	Bare Mud	0.38	0.67			0.54	0.78		
MLC	Sponges	0.75	0.55			0.8	0.37		
	Fine Det.	0.4	0.75			0.3	0.5		
	Coarse Det.	0.87	0.82	0.65	0.55	0.77	0.72	0.54	0.42
	SAV	0.69	0.52			0.67	0.48		
	Bare Mud	0.42	0.56			0.23	0.56		
OBIA	Sponges	0	0			1	0.28		
	Fine Det.	0.24	0.5			0.2	0.59		
	Coarse Det.	0.92	0.66	0.52	0.38	0.9	0.57	0.51	0.38
	SAV	0.55	0.92			0.55	0.72		
	Bare Mud	0.23	0.23			0.34	0.23		
TexAn	Sponges	0	0			0.13	0.05		
	Fine Det.	0.26	0.84			0.15	1		
	Coarse Det.	1	0.22	0.45	0.32	0.5	0.04	0.18	0.04
	SAV	0.49	0.8			0.45	0.16		
	Bare Mud	0.62	0.89			0	0		

Table A2. User, Producer and Overall accuracies for the different classification methods into four classes (obtained unifying sponges and SAV) for the 0.05 m and 0.2m grid resolution

Method	Class/Accuracy	005 m Grids				02 m Grids			
		Producer	User	Overall	kappa	Producer	User	Overall	kappa
Jenks	Sponges+SAV	0.88	0.79			0.81	0.72		
	Fine Det.	0.45	0.83	0.71	0.58	0.23	0.5	0.65	0.49
	Coarse Det.	0.9	0.56			0.95	0.56		
	Bare Mud	0.38	0.67			0.54	0.78		
MLC	Sponges+SAV	0.94	0.7			0.86	0.51		
	Fine Det.	0.39	0.75	0.73	0.61	0.3	0.5	0.58	0.42
	Coarse Det.	0.87	0.81			0.77	0.72		
	Bare Mud	0.42	0.56			0.23	0.56		
OBIA	Sponges+SAV	0.74	0.68			0.72	0.6		
	Fine Det.	0.24	0.5	0.61	0.43	0.2	0.58	0.55	0.36
	Coarse Det.	0.91	0.66			0.9	0.56		
	Bare Mud	0.22	0.22			0.33	0.22		
TexAn	Sponges+SAV	0.8	0.7			0.47	0.28		
	Fine Det.	0.26	0.83	0.58	0.42	0.19	1	0.26	0.07
	Coarse Det.	1	0.22			0.5	0.03		
	Bare Mud	0.62	0.89			0	0		

Table A3. User, Producer and Overall accuracies for the different classification methods into three classes (sponges + SAV, fine + coarse detritus, bare mud) for the 0.05 m and 0.2m grid resolution

Method	Class/Accuracy	005 m Grids				02 m Grids			
		Producer	User	Overall	kappa	Producer	User	Overall	kappa
Jenks	Sponges+SAV	0.88	0.79			0.81	0.72		
	Fine + Coarse Det.	0.95	0.91	0.83	0.72	0.8	0.82	0.77	0.61
	Bare Mud	0.38	0.67			0.54	0.78		
MLC	Sponges+SAV	0.94	0.7			0.86	0.51		
	Fine + Coarse Det.	0.81	0.98	0.81	0.68	0.78	0.89	0.68	0.49
	Bare Mud	0.42	0.56			0.23	0.56		
OBIA	Sponges+SAV	0.74	0.68			0.72	0.6		
	Fine + Coarse Det.	0.67	0.73	0.66	0.41	0.62	0.77	0.64	0.37
	Bare Mud	0.22	0.22			0.33	0.22		
TexAn	Sponges+SAV	0.8	0.7	0.76	0.59	0.47	0.28	0.59	0.17

Fine + Coarse Det.	0.76	0.8		0.62	0.91
Bare Mud	0.62	0.89		0	0

Table B1. Raw confusion matrices for the accuracy assessment at five thematic classes

J05	1. sponges	2. fine det.	3. coarse det.	4. sav	5. bare mud	n.classified pixels
1. sponges	**18**	0	0	0	4	**22**
2. fine det.	0	**10**	2	0	0	**12**
3. coarse det.	2	10	**18**	0	2	**32**
4. sav	0	2	0	**19**	4	**25**
5. bare mud	0	0	0	3	**6**	**9**
	20	**22**	**20**	**22**	**16**	**100**

J02	1. sponges	2. fine det.	3. coarse det.	4. sav	5. bare mud	n.classified pixels
1. sponges	**13**	1	1	5	2	**22**
2. fine det.	0	**6**	0	5	1	**12**
3. coarse det.	1	12	**18**	0	1	**32**
4. sav	0	7	0	**16**	2	**25**
5. bare mud	0	0	0	2	**7**	**9**
	14	**26**	**19**	**28**	**13**	**100**

MLC005	1. sponges	2. fine det.	3. coarse det.	4. sav	5. bare mud	n.classified pixels
1. sponges	**12**	0	0	6	4	**22**
2. fine det.	0	**9**	3	0	0	**12**
3. coarse det.	1	5	**26**	0	0	**32**
4. sav	2	6	1	**13**	3	**25**
5. bare mud	1	3	0	0	**5**	**9**
	16	**23**	**30**	**19**	**12**	**100**

MLC02	1. sponges	2. fine det.	3. coarse det.	4. sav	5. bare mud	n.classified pixels
1. sponges	**8**	2	1	4	7	**22**
2. fine det.	0	**6**	4	2	0	**12**
3. coarse det.	1	6	**23**	0	2	**32**
4. sav	0	3	2	**12**	8	**25**
5. bare mud	1	3	0	0	**5**	**9**
	10	**20**	**30**	**18**	**22**	**100**

37

OBIA005	1. sponges	2. fine det.	3. coarse det.	4. sav	5. bare mud	n.classified pixels
1. sponges	**0**	6	2	9	5	**22**
2. fine det.	0	**6**	0	4	2	**12**
3. coarse det.	1	5	**21**	5	0	**32**
4. sav	0	2	0	**23**	0	**25**
5. bare mud	0	6	0	1	**2**	**9**
	1	**25**	**23**	**42**	**9**	**100**

OBIA02	1. sponges	2. fine det.	3. coarse det.	4. sav	5. bare mud	n.classified pixels
1. sponges	**6**	9	0	4	3	**22**
2. fine det.	0	**7**	2	3	0	**12**
3. coarse det.	0	7	**18**	7	0	**32**
4. sav	0	6	0	**18**	1	**25**
5. bare mud	0	6	0	1	**2**	**9**
	6	**35**	**20**	**33**	**6**	**100**

TEXAN005	1. sponges	2. fine det.	3. coarse det.	4. sav	5. bare mud	n.classified pixels
1. sponges	**0**	8	0	13	1	**22**
2. fine det.	0	**10**	0	2	0	**12**
3. coarse det.	0	18	**7**	6	1	**32**
4. sav	0	2	0	**20**	3	**25**
5. bare mud	0	1	0	0	**8**	**9**
	0	**39**	**7**	**41**	**13**	**100**

TEXAN02	1. sponges	2. fine det.	3. coarse det.	4. sav	5. bare mud	n.classified pixels
1. sponges	**1**	20	0	1	0	**22**
2. fine det.	0	**12**	0	0	0	**12**
3. coarse det.	2	27	**1**	2	0	**32**
4. sav	2	18	1	**4**	0	**25**
5. bare mud	3	4	0	2	**0**	**9**
	8	**81**	**2**	**9**	**0**	**100**

38

Table B2. Raw confusion matrices for the accuracy assessment at four thematic classes

J05	1. sponges	2. fine det.	3. coarse det.	5. bare mud	n.classified pixels
1. sponges+sav	**37**	2	0	8	**47**
2. fine det.	0	**10**	2	0	**12**
3. coarse det.	2	10	**18**	2	**32**
5. bare mud	3	0	0	**6**	**9**
	42	**22**	**20**	**16**	**100**

J02	1. sponges	2. fine det.	3. coarse det.	5. bare mud	n.classified pixels
1. sponges+sav	**34**	8	1	4	**47**
2. fine det.	5	**6**	0	1	**12**
3. coarse det.	1	12	**18**	1	**32**
5. bare mud	2	0	0	**7**	**9**
	42	**26**	**19**	**13**	**100**

MLC005	1. sponges	2. fine det.	3. coarse det.	5. bare mud	n.classified pixels
1. sponges+sav	**33**	6	1	7	**47**
2. fine det.	0	**9**	3	0	**12**
3. coarse det.	1	5	**26**	0	**32**
5. bare mud	1	3	0	**5**	**9**
	35	**23**	**30**	**12**	**100**

MLC02	1. sponges	2. fine det.	3. coarse det.	5. bare mud	n.classified pixels
1. sponges+sav	**24**	5	3	15	**47**
2. fine det.	2	**6**	4	0	**12**
3. coarse det.	1	6	**23**	2	**32**
5. bare mud	1	3	0	**5**	**9**
	28	**20**	**30**	**22**	**100**

OBIA005	1. sponges	2. fine det.	3. coarse det.	5. bare mud	n.classified pixels
1. sponges+sav	**32**	8	2	5	**47**
2. fine det.	4	**6**	0	2	**12**
3. coarse det.	6	5	**21**	0	**32**
5. bare mud	1	6	0	**2**	**9**
	43	**25**	**23**	**9**	**100**

OBIA02	1. sponges	2. fine det.	3. coarse det.	5. bare mud	n.classified pixels
1. sponges+sav	**28**	15	0	4	**47**
2. fine det.	3	**7**	2	0	**12**
3. coarse det.	7	7	**18**	0	**32**
5. bare mud	1	6	0	**2**	**9**
	39	**35**	**20**	**6**	**100**

TEXAN005	1. sponges	2. fine det.	3. coarse det.	5. bare mud	n.classified pixels
1. sponges+sav	**33**	10	0	4	**47**
2. fine det.	2	**10**	0	0	**12**
3. coarse det.	6	18	**7**	1	**32**
5. bare mud	0	1	0	**8**	**9**
	41	**39**	**7**	**13**	**100**

TEXAN02	1. sponges	2. fine det.	3. coarse det.	5. bare mud	n.classified pixels
1. sponges+sav	**8**	20	1	0	**29**
2. fine det.	0	**12**	0	0	**12**
3. coarse det.	4	27	**1**	0	**32**
5. bare mud	5	4	0	**0**	**9**
	17	**63**	**2**	**0**	**82**

Table B3. Raw confusion matrices for the accuracy assessment at three thematic classes

J05	1. sponges	2. fine det.	5. bare mud	n.classified pixels
1 sponges+sav	**37**	2	8	**47**
2. fine det. + coarse det.	2	**40**	2	**44**
5. bare mud	3	0	**6**	**9**
	42	**42**	**16**	**100**

J02	1. sponges	2. fine det.	5. bare mud	n.classified pixels
1. sponges+sav	**34**	9	4	**47**
2. fine det. + coarse det.	6	**36**	2	**44**
5. bare mud	2	0	**7**	**9**
	42	**45**	**13**	**100**

MLC005	1. sponges	2. fine det.	5. bare mud	n.classified pixels
1. sponges+sav	**33**	7	7	**47**
2 fine det. + coarse det.	1	**43**	0	**44**
5. bare mud	1	3	**5**	**9**
	35	**53**	**12**	**100**

MLC02	1. sponges	2. fine det.	5. bare mud	n.classified pixels
1. sponges+sav	**24**	8	15	**47**
2. fine det. + coarse det.	3	**39**	2	**44**
5. bare mud	1	3	**5**	**9**
	28	**50**	**22**	**100**

OBIA005	1. sponges	2. fine det.	5. bare mud	n.classified pixels
1. sponges+sav	**32**	10	5	**47**
2. fine det. + coarse det.	10	**32**	2	**44**
5. bare mud	1	6	**2**	**9**
	43	**48**	**9**	**100**

OBIA02	1. sponges	2. fine det.	5. bare mud	n.classified pixels
1. sponges+sav	**28**	15	4	**47**
2. fine det. + coarse det.	10	**34**	0	**44**
5. bare mud	1	6	**2**	**9**
	39	**55**	**6**	**100**

TEXAN005	1. sponges	2. fine det.	5. bare mud	n.classified pixels

1. sponges+sav	**33**	10	4	**47**
2. fine det. + coarse det.	8	**35**	1	**44**
5. bare mud	0	1	**8**	**9**
	41	**46**	**13**	**100**

TEXAN02	**1. sponges**	**2. fine det.**	**5. bare mud**	**n.classified pixels**
1. sponges+sav	**8**	21	0	**29**
2. fine det. + coarse det.	4	**40**	0	**44**
5. bare mud	5	4	**0**	**9**
	17	**65**	**0**	**82**

Highlights

>We show that MBES can be used to explore extremely shallow (<10 m) and poorly known environments as tidal channels.

> We compare a set of image segmentation approaches for very-high resolution MBES data in very-shallow waters assessing pro and contra of each method.

>The unprecedented detail obtained through MBES and ground truth data allowed the discovery of ecologically noteworthy biogenic features such as sponges